How accurately do coupled climate models predict the leading modes of Asian-Australian monsoon interannual variability?

**Bin Wang · June-Yi Lee · I.-S. Kang · J. Shukla ·
J.-S. Kug · A. Kumar · J. Schemm · J.-J. Luo ·
T. Yamagata · C.-K. Park**

Abstract Accurate prediction of the Asian-Australian monsoon (A-AM) seasonal variation is one of the most important and challenging tasks in climate prediction. In order to understand the causes of the low accuracy in the current prediction of the A-AM precipitation, this study strives to determine to what extent the ten state-of-the-art coupled atmosphere-ocean-land climate models and their multi-model ensemble (MME) can capture the two observed major modes of A-AM rainfall variability–which account for 43% of the total interannual variances during the retrospective prediction period of 1981–2001. The first mode is associated with the turnabout of warming to cooling in the El Niño-Southern Oscillation (ENSO), whereas the second mode leads the warming/cooling by about 1 year, signaling precursory conditions for ENSO. The first mode has a strong biennial tendency and reflects

B. Wang (✉) · J.-Y. Lee
University of Hawaii/IPRC,
POST Building, Room 401,
1680 East-West Road, Honolulu, HI 96822, USA
e-mail: wangbin@hawaii.edu

I.-S. Kang · J.-S. Kug
Seoul National University, Seoul, South Korea

J. Shukla
George Mason University and COLA,
Calverton, MD, USA

A. Kumar · J. Schemm
NCEP/NOAA Climate Prediction Center,
Camp Springs, MD, USA

J.-J. Luo · T. Yamagata
FRCGC/JAMSTEC, Yokohama, Japan

C.-K. Park
APEC Climate Center, Busan, South Korea

the Tropical Biennial Oscillation (Meehl in J Clim 6:31–41, 1993). We show that the MME 1-month lead prediction of the seasonal precipitation anomalies captures the first two leading modes of variability with high fidelity in terms of seasonally evolving spatial patterns and year-to-year temporal variations, as well as their relationships with ENSO. The MME shows a potential to capture the precursors of ENSO in the second mode about five seasons prior to the maturation of a strong El Niño. However, the MME underestimates the total variances of the two modes and the biennial tendency of the first mode. The models have difficulties in capturing precipitation over the maritime continent and the Walker-type teleconnection in the decaying phase of ENSO, which may contribute in part to a monsoon "spring prediction barrier" (SPB). The NCEP/CFS model hindcast results show that, as the lead time increases, the fractional variance of the first mode increases, suggesting that the long-lead predictability of A-AM rainfall comes primarily from ENSO predictability. In the CFS model, the correlation skill for the first principal component remains about 0.9 up to 6 months before it drops rapidly, but for the spatial pattern it exhibits a drop across the boreal spring. This study uncovered two surprising findings. First, the coupled models' MME predictions capture the first two leading modes of precipitation variability better than those captured by the ERA-40 and NCEP-2 reanalysis datasets, suggesting that treating the atmosphere as a slave may be inherently unable to simulate summer monsoon rainfall variations in the heavily precipitating regions (Wang et al. in J Clim 17:803–818, 2004). It is recommended that *future reanalysis should be carried out with coupled atmosphere and ocean models*. Second, While the MME in general better than any individual models, the CFS ensemble hindcast outperforms the MME in terms of the biennial tendency and the amplitude

of the anomalies, suggesting that the improved skill of MME prediction is at the expense of overestimating the fractional variance of the leading mode. Other outstanding issues are also discussed.

1 Introduction

While the detailed evolution of weather events may not be predictable beyond the span of a few days to 2 weeks due to the chaotic internal dynamics of the atmospheric motion (Lorenz 1965), the time or space averages of the atmospheric variables, or the statistical behavior of weather, may be predictable over timescales of a season or longer due to the interactions between the atmosphere and the more slowly varying oceans and land surface properties. The climate predictability, therefore, critically depends on the nature of the slow coupled physical processes. In the tropical Pacific, the sea surface temperature, surface winds, and precipitation are tightly coupled (Bjerknes 1969); and to a large extent, the climate variations in the region are determined by slow oceanic dynamical processes (Cane et al. 1986; Zebiak and Cane 1987). For this reason, El Niño-Southern Oscillation (ENSO) and its global impacts is perhaps the most predictable phenomenon in the Earth's climate system.

In contrast with the tropical Pacific climate, dynamical model simulation, and seasonal prediction of the Asian monsoon interannual variability in rainfall have been a major challenge (Sperber and Palmer 1996; Goswami 1998; Gadgil and Sajani 1998). Sperber and Palmer (1996) evaluated performances of 32 atmospheric general circulation models (AGCMs) that participated in the Atmospheric Model Intercomparison Project (AMIP). These models show little or no accuracy in predicting the all-Indian rainfall from 1979 to 1988 except during the 1987 El Niño and the 1988 La Niña. Wang et al. (2004) assessed performances of the ensemble simulations of Asian-Australian Monsoon (A-AM) anomalies in 11 AG-CMs during the unprecedented El Niño period from September 1996 to August 1998. The 11-model ensemble simulation of anomalous Asian summer rainfall patterns in the A-AM region (30°S–30°N, 40°E–160°E) shows a map correlation coefficient of about 0.45, which is considerably lower than its counterpart in the El Niño region (in which the map correlation coefficient is about 0.8). Examination of potential predictability of five AGCMs' multi-model

ensemble (MME) hindcast for a 21-year period confirmed that when the models are forced by observed sea surface temperature (SST), they are unable to effectively predict Asian-Pacific summer monsoon rainfall (Wang et al. 2005).

The difficulty in simulating and predicting the Asian summer monsoon's seasonal rainfall is in part due to limitations in predicting the monsoon's intrinsic internal dynamics. Using the Geophysical Fluid Dynamics Laboratory AGCM, Goswami (1998) hypothesized that the contribution of ENSO to the interannual variability in Indian monsoon region is comparable to the regional scale fluctuations that arise from an internal oscillation unrelated to SST anomalies. Thus, the models' low prediction ability in the Asian summer monsoon region may be due to chaotic dynamics associated with synoptic to intraseasonal fluctuations and/or an unpredictable part of the interaction with the land-surface or ocean process. But, there are other potential sources that might be prohibiting practical monsoon predictability. The role of other low-frequency (LF) boundary forcing, such as Eurasian and Himalayan snow cover, is still unclear.

One of the factors that limit the predictability is related to the strategies of the AGCM-alone simulation and so-called "two-tier" prediction. Sperber and Palmer (1996) noted that the correct mean state were more likely to correctly capture the interannual variability of tropical precipitation. In addition, Turner et al. (2005) showed that improved accuracy in prediction of atmospheric teleconnection patterns associated with ENSO requires the accurate prediction of the climatological mean state. But, the coupled atmosphere–ocean models often have deficiencies in reproducing good climatology. In order to better predict climate anomalies associated with ENSO teleconnection patterns, Bengtsson et al. (1993) proposed a two-tier approach, in which SST was first predicted by using coupled models, and then the atmospheric anomalies were predicted by using atmospheric models forced by the predicted SST. Recent research using coupled ocean–atmosphere models suggests that the prediction of summer monsoon precipitation requires investigators to take into account the local monsoon–warm pool ocean interactions (Wang et al. 2003, 2004; Wu and Kirtman 2005; Kumar et al. 2005). It has been shown that the poor performance of atmospheric models forced by observed SST in simulating the Asian summer monsoon's variability is partially attributed to the experimental design, in which the atmosphere is forced to respond passively to the specified SSTs, while in nature, the SSTs result in part from the atmospheric forcing (Wang et al. 2004). In the absence of the monsoon–ocean interaction, all models yield positive SST-rainfall correlations that are at odds with observations in the heavily precipitating summer monsoon region (Wang et al. 2005). Therefore, to assess the monsoon's predictability, it is

desirable to use coupled atmosphere–ocean models or a one-tier prediction system.

The accuracy of seasonal prediction can be constrained by errors in observation and errors in determining the initial states of the atmosphere and ocean, and can also be limited by the uncertainties in a model's physical parameterization of the effects of unresolved processes on unresolved scales. An ensemble prediction starting from different initial conditions provides a way of distinguishing the ensemble mean, which is believed to be related to climate signal, and determining the deviation from the ensemble mean, which is regarded as a measure of the noise and uncertainty due to internal chaotic dynamics (Shukla 1981; Rowell et al. 1995; Shukla et al. 2000). To further reduce the errors associated with the uncertainties in one model's physical parameterizations, multiple models were used in this study, drawing upon the *assumption* that anomaly errors in various model solutions are spread randomly. Although systematic errors in climatological mean states such as cold tongue bias, excessive trade winds, and double ITCZ, are similar in many models, our recent analysis found that the *anomaly errors* are of quite diverse among models. To obtain a consensus view about the current status of CGCMs, a simple composite method was used to compute a MME. The MME is an effective way to aggregate and synthesize multi-model forecasts. It has been recognized that in MME the ensemble average reduces the noise present in the individual forecasts, increasing the correlations, and reducing the systematic error (Krishnamurti et al. 1999; Doblas-Reyes et al. 2000; Palmer et al. 2000). In the following assessment of the summer monsoon predictability, we will analyze the MME results in order to establish a better estimate of the practical predictability.

Determining the predictability of the summer monsoon and identifying the sources of predictability are of central importance in seasonal prediction and in forecasting the potential uncertainties associated with the prediction. How to determine climate predictability in a coupled model hindcast remain elusive. We propose that the distinguished major modes of the A-AM interannual variations may represent or provide a measure for the predictable part of the variability. Furthermore, the models' performances in capturing these major modes may be related to their seasonal prediction skills. Therefore, it is important to (1) determine what the major modes of A-AM interannual variability are, (2) assess how well the state-of-the-art coupled climate models capture the leading modes of the A-AM interannual variability, and (3) determine how the models' performances in capturing these leading modes are related to the seasonal prediction skills. These are the major purposes of the present study.

Our analysis will primarily focus on precipitation, because precipitation is the most important variable for seasonal prediction and because it is also the most difficult variable for seasonal prediction. Examination of precipitation prediction is the most rigorous test for climate models. Retrospective forecasts use updated initial conditions. The influence of initial conditions is expected to make CGCM more realistically predict the A-AM anomalies compared to the previous simulations in the coupled long integrations.

2 The models, data, and analysis procedure

2.1 The models and data

The models that are examined in this study are ten fully coupled atmosphere–ocean–land seasonal prediction systems that come from the following two international projects: "**D**evelopment of a **E**uropean **M**ulti-model **E**nsemble system for seasonal to in**TER**annual prediction" (DEMETER) (Palmer et al. 2004) and the Asia-Pacific Economic Cooperation Climate Center/Climate Prediction and Its Application to Society (APCC/CliPAS) (Wang et al. 2007b). Table 1 presents a brief summary of each model. For more details of the models, the readers are referred to the relevant literatures cited in the Table 1. These models include seven models from DEMETER, which come from European Centre for Research and Advanced Training in Scientific Computation (CERFACS), European Centre for Medium-Range Weather Forecasts (ECMWF), Instituto Nazionale di Geofisica e Vulcanologia (INGV), Laboratoire d'Océanographie Dynamique et de Climatologie (LODYC), Centre National de Recherches Meteorologiques (Meteor-France), the UK Met Office, and Max Planck Institute for Meteorologie (MPI). Also included are three coupled models from APCC/CliPAS: the Frontier Research Center for Global Change (FRCGC), the National Center for Environmental Prediction (NCEP), and the Seoul National University (SNU).

All selected models have retrospective forecast (hindcast) for the common 21-year period of 1981–2001 with 6- to 9-month integrations for 6–15 members starting from different initial conditions for four seasons. The hindcasts are initialized in February 1, May 1, August 1, and November 1 except the CFS model, in which the 15 atmospheric initial conditions were taken on the 9, 10, 11, 12, 13, 19, 20, 21, 22, and 23 of the month prior to the target month, and on the second-to-last day of the previous month, as well as the first-to-third days of the targeting month (Saha et al. 2006).

In the present study, we focus on evaluating 1-month lead *seasonal* forecast. Suppose the forecast was initialized on February 1, the 1-month lead seasonal prediction means the average of predicted March, April, and May means. The CFS hindcast was issued every month with an

Table 1 Description of ten coupled models used in this study

Institute	Model name	AGCM	OGCM	Ensemble member	Reference
CERFACE	CERFACE	ARPEGE	OPA 8.2	9	Deque (2001)
		T63 L31	2.0° lat × 2.0° lon L31		Delecluse and Madec (1999)
ECMWF	ECMWF	IFS	HOPE-E	9	Gregory et al. (2000)
		T95 L40	1.4° lat × 0.3–1.4° lon L29		Wolff et al. (1997)
INGV	INGV	ECHAM4	OPA 8.2	9	Roeckner et al. (1996)
		T42 L19	2.0° lat × 2.0° lon L31		Madec et al. (1998)
LODYC	LODYC	IFS	OPA 8.0	9	Gregory et al. (2000)
		T95 L40	182GP × 152GP L31		Delecluse and Madec (1999)
Meteo-France	Meteo-France	ARPEGE	OPA 8.0	9	Deque (2001)
		T63 L31	182GP × 152GP L31		Madec et al. (1997)
MPI	MPI	ECHAM5	MPI-OM1	9	Roeckner et al. (1996)
		T42 L19	2.5° lat × 0.5–2.5° lon L23		Marsland et al. (2002)
UKMO	UKMO	HadAM3	GloSea OGCM	9	Pope et al. (2000)
		2.5 × 3.75L19	1.25° lat × 0.3–1.25° lon L40		Gordon et al. (2000)
FRCGC	SINTEX-F	ECHAM4	OPA 8.2	9	Luo et al. (2005)
		T106 L19	2° cos(lat) × 2° (lon) L31		
NCEP	CFS	GFS	MOM3	15	Saha et al. (2006)
		T62 L64	1/3° lat × 5/8° lon L27		
SNU	SNU	SNU	MOM2.2	6	Kug and Kang (2007)
		T42 L21	1/3° lat × 1° lon L40		

integration time of 9 months. Thus, the CFS data make it possible to assess the predictability as a function of forecast lead time and the impact of initial conditions. In this hindcast that is initiated from each month, the first monthly mean of the forecast is defined as the 0-month lead because three ensemble members were initialized in the first 3 days of the target month. Similarly, the second monthly mean is defined as the 1-month lead. The remaining lead times are defined analogously.

2.2 Data

The Climate Prediction Center Merged Analysis of Precipitation (CMAP) data set (Xie and Arkin 1997) and the Global Precipitation Climatology Project (GPCP) data (Adler et al. 2003) were used as verification datasets. For comparison, two reanalysis datasets—the NCEP/DOE AMIP II Reanalysis ("NCEP-2") data (Kanamitsu et al. 2002), which is essentially the NCEP/NCAR reanalysis with bugs fixed, and the ECMWF 40-year Reanalysis ("ERA-40") data (Uppala et al. 2005)—were also used to assess their leading modes of precipitation over the A-AM monsoon region. The observational 850 hPa wind fields are obtained from NCEP-2, and the observational SST data are obtained from the improved Extended Reconstructed SST Version 2 (ERSST V2) data (Smith and Reynolds 2004).

2.3 Analysis procedure

The year-to-year variation in the vast A-AM region exhibits enormous regional differences and depends strongly on the phase of the annual cycle (Meehl 1987). Based on this physical consideration, Wang and An (2005) have put forth a Season-reliant Empirical Orthogonal Function (S-EOF) analysis method to distinguish modes of variability that evolve with the seasons. Their S-EOF analysis of the Indo-Pacific SST anomalies yielded two statistically significant leading modes that are not obtainable by using conventional EOF analysis. The two leading modes represent LF and Quasi-Biennial (QB) modes, which are distinguished from each other in their seasonal evolution, spatial structure of the fractional variance, and interdecadal variation and trend. The differences between the S-EOF and the extended (Weare and Nasstrom 1982) and cyclostationary EOF (Kim 2002) analyses were discussed in Wang and An (2005). The advantages of the S-EOF compared to the conventional EOF analysis and why the S-EOF was used to derive the major modes were discussed in detail in Wang et al. (2007a).

The purpose of the S-EOF is to depict seasonally evolving anomalies throughout a full calendar year. Here, we adopted the concept of the "monsoon year" (Yasunari 1991), which spans from the summer (June, July, and August) of Year 0, or "JJA(0)," to the spring (March,
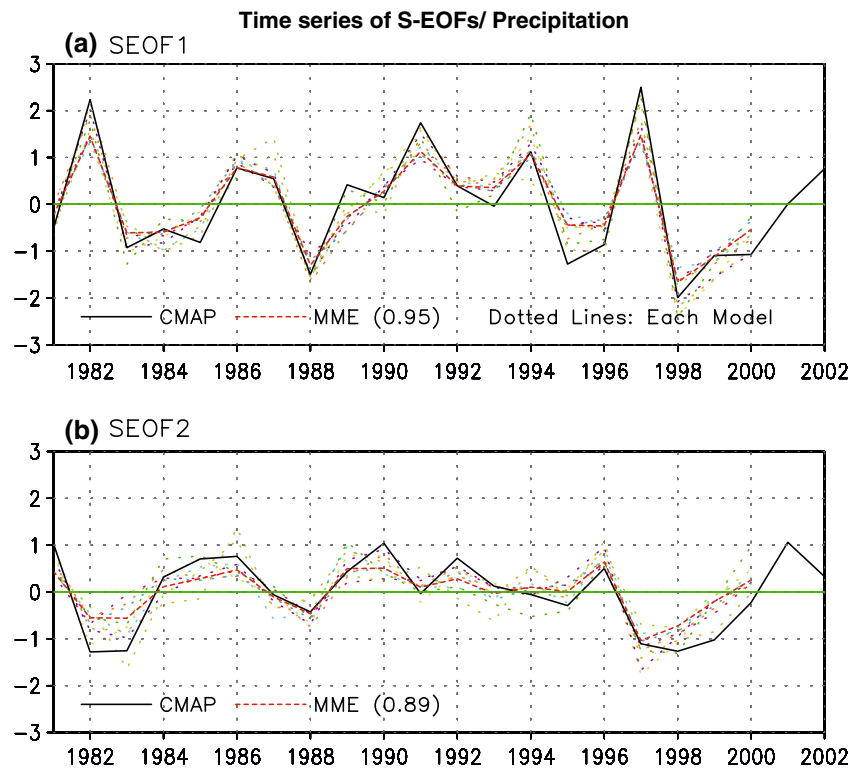
April, and May) of the following year (Year 1), or "MAM(1)". For this purpose, a covariance matrix was constructed using four consecutive seasonal mean anomalies for each year; in other words, the anomalies for JJA(0), SON(0), DJF(0/1), and MAM(1) were treated as a "yearly block" that is labeled Year 0—the year in which the sequence of anomalies commences. After the EOF decomposition is finished, the yearly block is then divided into four consecutive seasonal anomalies, to obtain a seasonally evolving pattern of the monsoon anomalies in each monsoon year for each eigenvector.

We have applied the S-EOF analysis to both observed and predicted seasonal mean precipitation anomalies, which are the departures from the mean annual cycle derived from the period of 1981–2001. In the present study, we consider the A-AM region as extending from 40°E to 160°E, and from 30°S to 40°N, which covers South Asia and Australia as well as nearly the entire Indo-Pacific warm pool region.

3 Observed leading modes of the Asian-Australian monsoon system

The S-EOF analysis of CMAP precipitation seasonal anomalies (1981–2002) yields two statistically distinguished leading modes, which account for 30.1 and 13.1% of the total variance in precipitation anomalies, respectively. Figure 1 shows the time series of the principal

component (PC) of the first and second S-EOF mode. The PCs of the two leading modes are closely related to ENSO as measured by the NINO 3.4 SST anomalies. To examine their relationship with ENSO, the lead-lag correlation coefficients between the two PCs and the seasonal NINO 3.4 SST anomalies are presented in Fig. 2. Note that the A-AM precipitation seasonal anomaly from JJA(0) to the next MAM(1) is centered on November and December of Year 0, thus, the PCs have a yearly resolution centered on November–December of each year. The observed first mode shows a maximum positive correlation coefficient that exceeds 0.9 with NINO 3.4 SST anomaly in DJF(0/1). Since El Niño events normally mature toward the end of the calendar years (Rasmussen and Carpenter 1982), the result in Fig. 2a indicates that the first S-EOF mode concurs with El Niño turnaround. On the other hand, the observed second mode shows a maximum correlation coefficient (about 0.75) leading El Niño by about 1 year, suggesting it may provide a precursory signal for ENSO onset (Fig. 2b).

Figure 3a shows the seasonal evolutions of the spatial patterns of CMAP precipitation anomalies which were linearly regressed against the corresponding first PC in an enlarged domain including the tropical Indo-Pacific Ocean. Also shown are linearly regressed patterns of the NCEP-2 850 hPa wind anomalies (vectors) against the first PC. We display the regressed anomalies with statistically significant level more than 90% for both precipitation and wind.
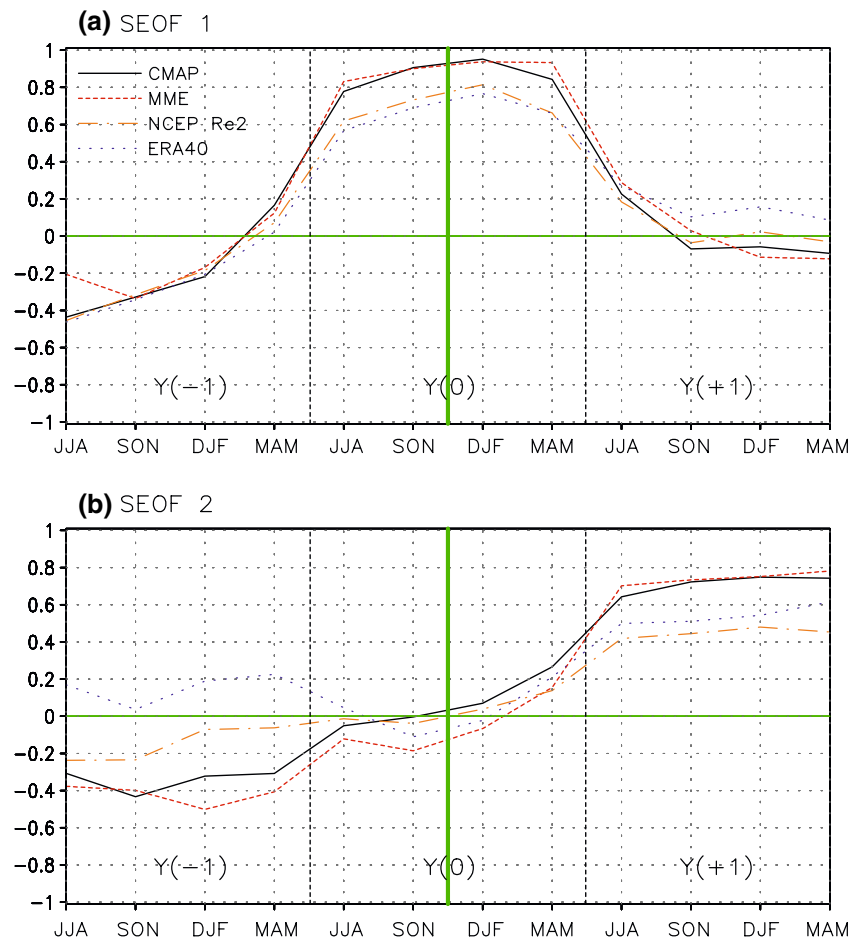
In JJA(0), large-scale suppressed convections are located over the maritime continent and the equatorial eastern Indian Ocean. The dry anomalies extend northwestward to the southern Indian subcontinent and the Arabian Sea. Enhanced rainfall is found over the equatorial western Pacific. The wet anomalies also extend northwestward to the Philippine Sea, the northern South China Sea, and the head of the Bay of Bengal. On the other hand, the precipitation along the East Asian monsoon front (Maiyu or Baiu) weakens. Associated with the anomalous convection patterns, an anomalous anticyclone ridge extends from the maritime continent to the southern tip of India, with enhanced monsoon westerlies extending from India to the western Pacific.

During SON(0), the dry anomalies over the maritime continent intensify and expand northward and eastward, covering the Philippine archipelago and the entire tropical South Asia and northern Australia; meanwhile, the western Indian Ocean becomes wetter than normal. The corresponding southern Indian Ocean (SIO) anticyclonic anomalies and the zonal wind divergence around the maritime continent are both well established. This pattern has been recognized as associated with the Indian Ocean

zonal (or dipole) SST mode (Saji et al. 1999; Webster et al. 1999). From the SON season to the DJF season, the entire anomalies move slowly eastward with the most suppressed convection shifting to the Philippine Sea. A new anticyclonic anomaly forms over the Philippine Sea. The East Asian winter monsoon weakens, but precipitation in southern China increases.

From DJF to the next MAM, the dry anomalies decay rapidly and move further eastward with a dry center occurring in the equatorial western Pacific. The SIO and Western North Pacific (WNP) anticyclones remain, but they weaken. The evolution of precipitation anomalies reflects their association with ENSO turnaround. Wang et al. (2003) pointed out that the remote El Nino forcing, monsoon–warm pool interaction, and the regulation of the monsoon annual cycle are three fundamental factors that give rise to the leading mode.

Figure 3b shows spatial patterns of the second S-EOF mode, which has not been documented previously. In SON(0), the fall prior to the El Niño development year, the WNP precipitation and the cyclonic circulation anomaly pattern shift equatorward from their positions during the previous summer, and the convective dipole in the

Fig. 3 Spatial patterns of the linear regression fields of seasonal CMAP precipitation anomalies (*color shading*, units of mm day^{-1}) and NCEP-2 850 hPa wind anomalies (*vectors*, unit of ms^{-1}) against the corresponding first principal component from JJA(0) to MAM (1). **b** Same as in (**a**) except for the second S-EOF mode. The regressed anomalies with more than 90% significant level are displayed for both precipitation and winds
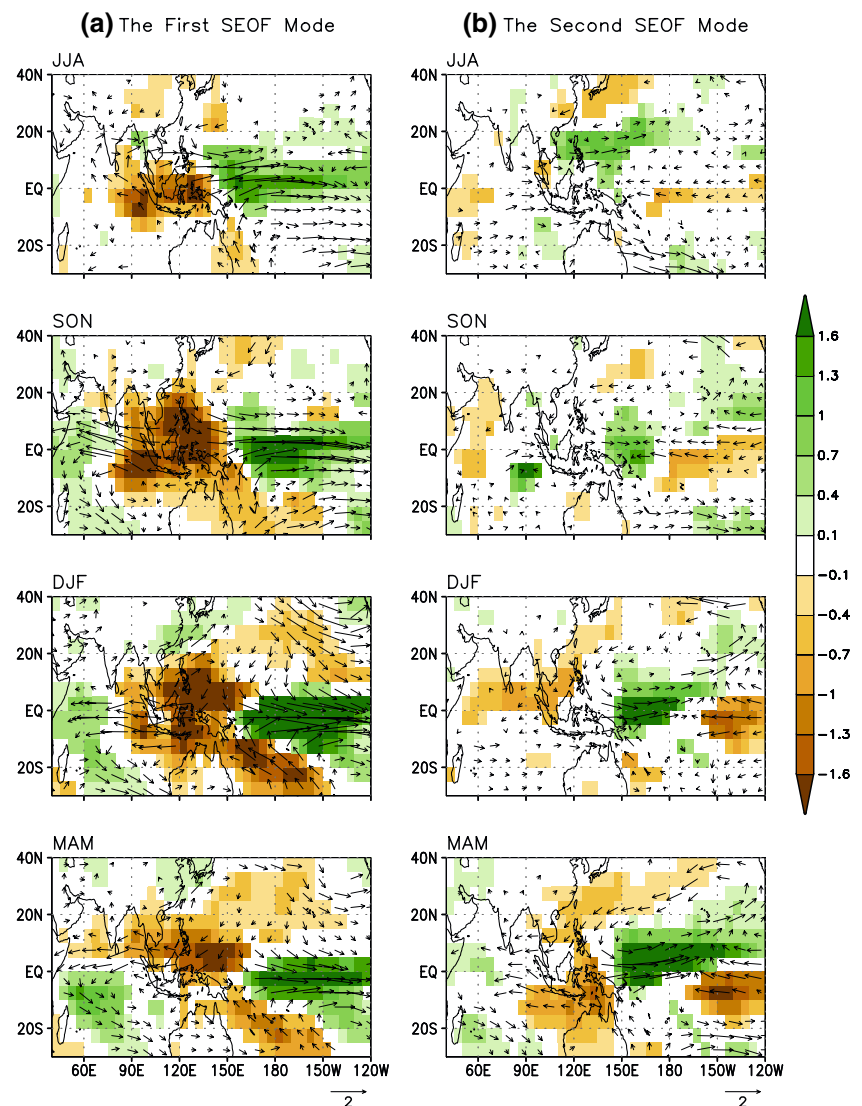
equatorial Indian Ocean intensifies. In the ensuing DJF and MAM, the WNP anomalous cyclone and associated equatorial westerly anomalies further strengthen, dominating the entire western Pacific region. At the same time, dry anomalies develop in the northern Indian Ocean and Southeast Asia in DJF(0/1) and over the eastern Indonesia and northern Australia in MAM(1). The anomalous pattern in MAM (1), such as the weakened trades over the western-central Pacific, is a robust precursor for El Niño development; it then evolves into a mature El Niño event in the central-eastern Pacific two or three seasons later.

Thus, an interesting precursory feature in the year prior to an ENSO event is that a large-scale cyclonic anomaly forms over the WNP in the summer to fall seasons prior to a year in which El Niño develops, followed by a continuous southeastward movement and strengthening through the following fall, winter, and next spring. This feature agrees well with the results of Wang (1995) who pointed out that this pattern has occurred since the late 1970s. This feature (change in ENSO-monsoon relationship) concurs with the late seventies climate shift in the North Pacific and changes in ENSO properties.

4 The major modes of A-AM variability in the MME prediction

In this section, we first evaluate the skill of the 1-month lead prediction of seasonal precipitation anomalies made by the ten one-tier models against two observed leading modes, then compare them with those derived from the two reanalysis datasets in order to fully appreciate the models' skill. The last part of this section discusses major deficiencies with the MME.
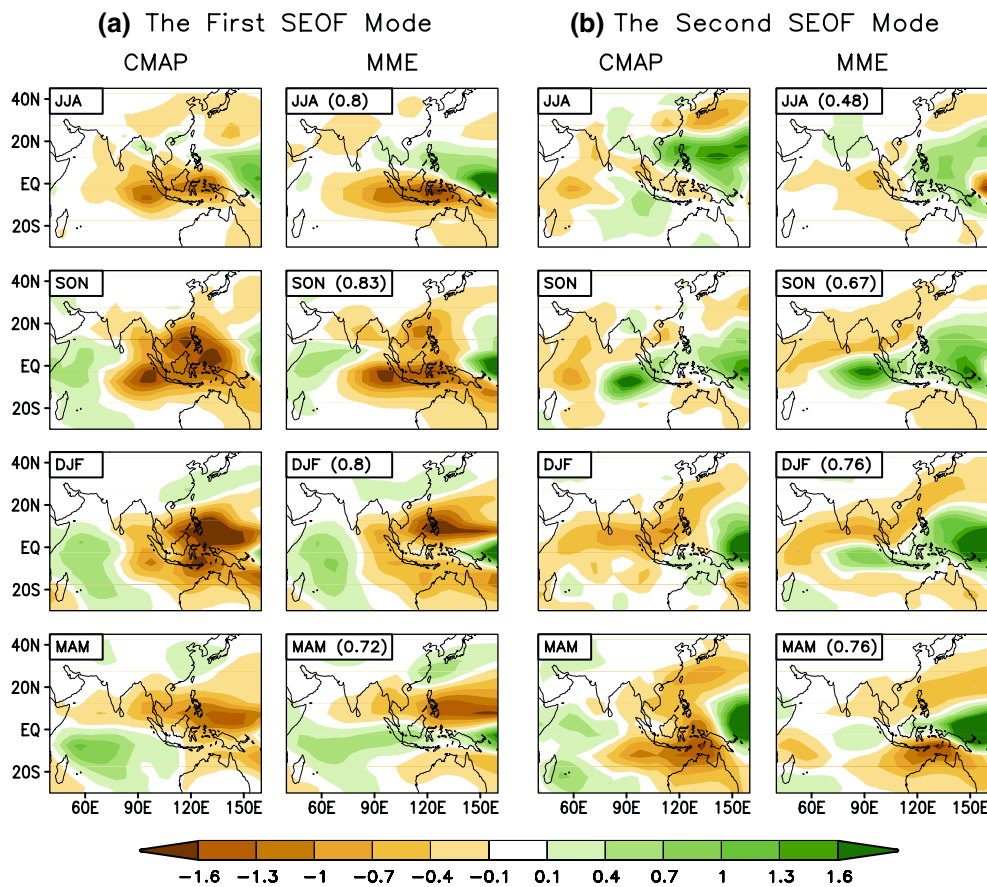
Fig. 4 **a** Comparison of the spatial patterns of the first S-EOF eigenvector of seasonal precipitation anomalies obtained from CMAP observation, CliPAS and DEMETER MME predictions. **b** The same as in (**a**) except for the second S-EOF mode. The numbers in the right upper corners indicate pattern correlation coefficients between observation and the corresponding prediction

4.1 The principal components and spatial patterns of the MME

Included in Fig. 1 are the temporal correlation coefficients between the observed and MME-predicted PC time series (0.95 for the first S-EOF mode and 0.89 for the second mode). Thus, the MME system reproduced the temporal variations of the observed first and second modes very well. Further, Fig. 2 indicates that the MME forecasts capture, with high fidelity, the lead-lag correlations between ENSO and the two leading modes, or the overall relationship between ENSO and A-AM. For the second mode, although ERA-40 only shows a positive correlation at −1 year, the difference between the two reanalysis results is not statistically significant because the absolute values of the correlation coefficients are small. Changing sign of correlation between −1 and +1 year means a quasi-4 year periodicity. Thus, the result here means that in ERA-40, the second mode has periodicity longer than 4 years.

The MME's hindcast also faithfully reproduces the major spatial distributions of the two observed leading modes of the interannual variability of A-AM seasonal precipitation (Fig. 4). This is important because a realistic temporal evolution doesn't warrant the corresponding spatial patterns are realistic. The current evaluation method relies on the fact that the S-EOF spatial patterns from the observation and models are quite similar. For the first S-EOF mode (Fig. 4a), the anomalous patterns from JJA(0) to DJF(0/1) are very well reproduced, with the anomaly pattern correlation coefficients being over 0.80. Larger discrepancies are found during the MAM (1) season over the western equatorial Pacific and the maritime continent, suggesting that during the decaying phase of ENSO, the models have deficiencies in capturing the austral fall monsoon precipitation over the maritime continent and the Walker-type teleconnection. This may lead to a drop of prediction skill across the boreal spring. The poor ability in capturing the austral fall monsoon precipitation could also be related to the poor persistence in seasonal evolution, i.e., a communication gap between Australian and Asian monsoon systems in austral fall prior to the onset of the Asian summer monsoon (Hung et al. 2004).

For the second mode (Fig. 4b), the anomaly patterns from SON(0) to MAM(1) are reproduced reasonably well

with map correlation coefficients ranging generally from 0.67 to 0.76. However, the JJA(0) pattern was poorly predicted. This indicates that about 1.5 years prior to the mature phase of ENSO, the monsoon variability is difficult to reproduce in the MME. The reason is conceivably due to the lack of significant SST anomaly forcing or due to the low predictability of the bereal summer monsoon in the transitional phase of ENSO. Since from boreal fall to spring, i.e., SON(0), DJF(0/1), and MAM(1), the anomaly patterns of the second mode are predicted well, the second mode of the MME shows a potential to capture the precursors of ENSO in the A-AM domain about 15 months prior to the maturation of a strong El Niño.

4.2 Comparison of the MME forecast with reanalysis

In order to appreciate the success of the MME's hindcast, it is useful to compare the coupled climate models' MME hindcast with the two reanalysis datasets, ERA-40 and NCEP-2. For this purpose, we used both anomaly pattern correlation and temporal correlation coefficients to assess the skills for the spatial pattern (Fig. 5a) and PC (Fig. 5b) of the first two leading modes. Note that the correlation coefficients, to a large extent, reflect the root mean square error very well (figure not shown).

In Fig. 5, the CMAP is used as the baseline for comparison. The other observed dataset, GPCP, is extremely well correlated with CMAP in general (Fig. 5). The dissimilarity between GPCP and CMAP provides additional information about the uncertainties in the observation due to the errors in estimation of tropical precipitation using different sources of satellite measurements and retrieval methods.

Of surprise is that the leading modes derived from the MME predictions are in general better or at least comparable to those derived from the two reanalysis datasets. In terms of the spatial pattern (Fig. 5a), the MME prediction of the first mode is significantly better than the corresponding one in the NCEP-2 and slightly better than that in ERA-40; for the second mode, the MME is considerably better than ERA-40 and slightly better than NCEP-2. In terms of temporal evolution (Fig. 5b), the ten-model MME shows considerably higher temporal correlation coefficients than the two reanalyses for both leading modes. Note also that the MME outperforms each individual model's ensemble. However, one member model has poor performance, with a map correlation coefficient of about 0.3–0.4 for the two leading modes. Additional calculation shows that even excluding that poorest model the MME performance remains about the same.

4.3 The weakness of the MME prediction

While the MME's prediction captures the spatial pattern and temporal evolution better than reanalysis, the standard deviations (amplitudes of spatial variability) in the MME prediction are significantly lower than those in the reanalyses for both modes (not shown), suggesting that the MME tends to underestimate the total variance. Thus, the MME improves the pattern and temporal correlation (compared to each individual model) at the expense of reducing the amplitude of the anomalies. Therefore, artificially boosting the temporal amplitudes of the two leading modes predicted by the MME may lead to reduced root mean square errors and could improve the forecasts.
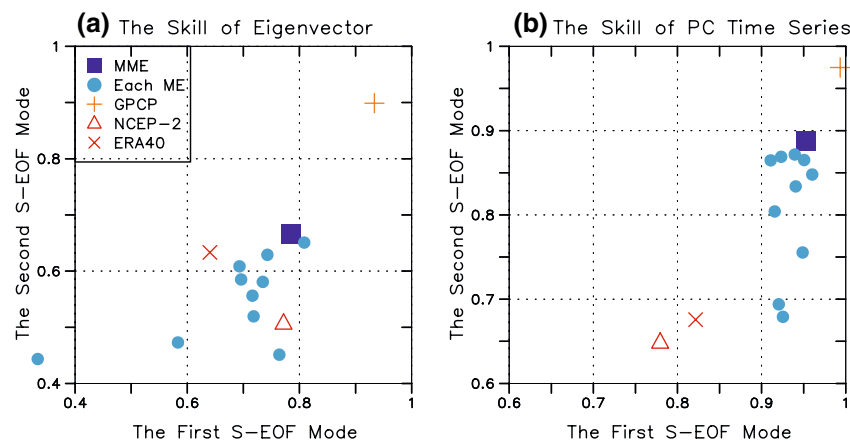

Fig. 5 Comparison of the performances of the MME and individual predictions, GPCP estimate, and two (NCEP-2 and ERA-40) reanalyses against the two observed (CMAP) dominant S-EOF modes of seasonal mean precipitation anomalies. The *abscissa* and *ordinate* represent, respectively, correlation coefficients between the observed and predicted (reanalyzed) anomalies for the first and second modes. The *left panel* is for the spatial correlation skill of the eigenvector, and the *right panel* is for the temporal correlation skill of the principal component

Figure 6 shows the percentage variance accounted for by the first six eigenvalues of the S-EOF analysis of the A-AM precipitation. Shown also is the unit standard deviation of the sampling errors associated with each eigenvalue's percentage variance. According to the rule of North et al. (1982), the first two observed leading modes are well distinguished from each other and from the rest of the S-EOFs in terms of the sampling error bars. Hence, they are both statistically distinguishable modes. Of interest is that the first two modes derived from the MME prediction have similar levels of statistical significance as the observed counterparts. However, the fractional variance of the first S-EOF mode derived from the MME prediction is considerably higher than its observed counterpart. The result indicates that the MME well produces the first two distinguished leading modes, but it tends to exaggerate the fractional variance of the first mode while reducing the variances of the higher modes. The MME is less noisy, because the higher modes are considered to reflect unpredictable noises. It is also found that the CFS 1-month lead seasonal hindcast yields a more realistic fractional variance for the first S-EOF (40% of total variance) than the MME counterpart (59.2%), suggesting that the MME tends to smooth out higher modes and thus overestimate the fractional variance of the leading mode compared with the individual models.

Figure 7 shows the power spectrum density distributions and corresponding red noise of the first and second PC time series. The red noise curve is derived from the first order of auto regressive (AR1) process with confidence level of 0.05. In the observation, the first mode has a major spectral peak at 2.5 years and a minor peak around 4–6 years. The MME captures the LF (4- to 6-year) peak reasonably well, but essentially fails in reproducing the QB component (left panels in Fig. 7). In the second mode, the observation and the MME prediction all show a LF spectral peak around 5 years, but the predicted variances are much smaller than the observed (right panels in Fig. 7). These results confirm that the amplitude of MME prediction needs to be corrected. It is also found that the PCs of the CFS 1-month lead seasonal hindcast are more realistic than the ten-model MME's PC spectra (not shown), suggesting that the MME tends to reduce the biennial tendency of the leading monsoon mode.
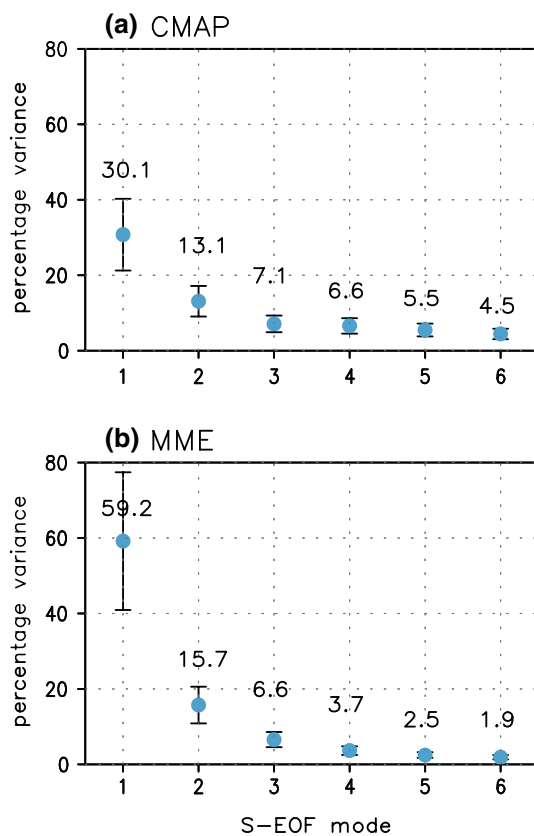

Fig. 6 Percentage variance (%) explained by the first six S-EOF modes of seasonal precipitation anomalies obtained from **a** CMAP and **b** MME prediction. The *bars* represent one standard deviation of the sampling errors
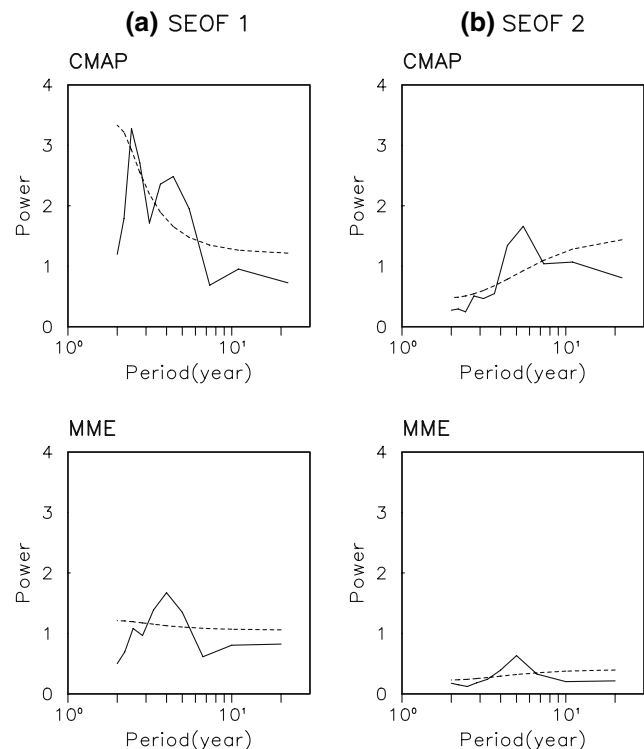

Fig. 7 The power spectrum density (*solid line*) and red noise (*dashed line*) of **a** the first (*left-hand panels*) and **b** the second (*right-hand panels*) S-EOF principal component of seasonal precipitation anomaly obtained from CMAP observation (*upper panels*) and from MME prediction (*lower panels*)
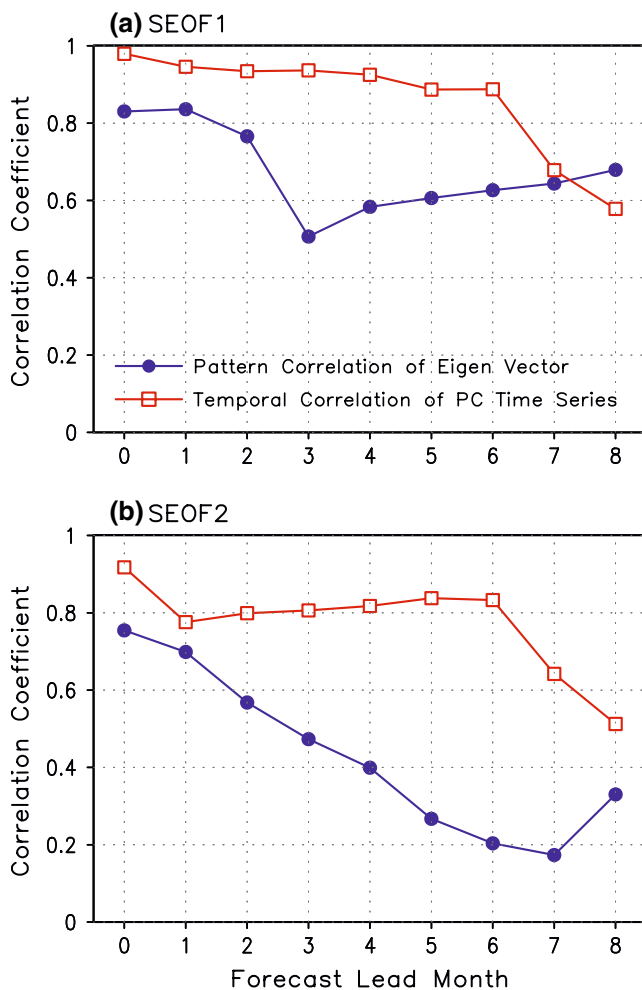
Fig. 8 a Dependence of correlation skills on forecast lead time for the seasonal prediction of the first S-EOF mode in Asian-Australian monsoon rainfall made by the NCEP CFS model. The *red curve* represents the anomaly pattern correlation coefficient between the observed and predicted eigenvector. The *blue curve* denotes the temporal correlation coefficient between the observed and predicted principal components. **b** The same as in (**a**) except for the second S-EOF mode

5 Forecast leading modes as function of lead time: CFS assessment

CFS retrospective hindcast was made with 15 members that were initialized before the 4th day of each calendar month. Each ensemble mean covered a 9-month prediction. Thus, it is possible to evaluate the prediction skill with lead times from 0 to 8 months. This allows us to examine how the forecast skills vary with the lead time, which measures the predictability of the A-AM precipitation anomalies in terms of the two leading modes.

Figure 8 shows how hindcast correlation skill varies with lead time in predicting the spatial patterns and temporal evolution (PCs) of the two leading modes of precipitation variability made by the CFS forecast. For the

first mode, the temporal correlation between the observed and predicted PC remains about 0.9 until the 6-month lead, when it drops significantly afterward (Fig. 8a). The anomaly pattern correlation coefficient between the observed and predicted spatial patterns decreases from 0.83 at 0-month lead to 0.68 at the 8-month lead. However, the decrease is not monotonic, rather, it exhibits a minimum at the 3-month lead (correlation coefficient of 0.51) then recovers gradually. Why does the skill show a minimum in the 3-month lead prediction?

Examination of the seasonal evolving anomaly patterns shown in Fig. 9 indicates that the skills are low for JJA(0) prediction with a 3- and 5-month lead. The drop of skill in the 3- and 5-month lead forecasts of the JJA(0) anomalies means that when the model starts its prediction in January through March, the skill for predicting the summer precipitation anomaly is low. Thus, the drop in skill seen in Fig. 8a suggests a "Spring Prediction Barrier" (Webster and Yang 1992) in A-AM seasonal forecast. Similarly the low skill for prediction of SON(0) with a 5-month lead also means a SPB. Examination of these models' performances reveals that the MME has a clear SPB in the prediction of NINO 3.4 SST anomalies (refer to Fig. 1. of Saha et al. 2006). This monsoon SPB in coupled models is, therefore, likely associated with the SPB in the models' ENSO prediction.

For the second mode, the temporal skill is similar to the first mode, but the spatial patterns show a steady decline of the correlation scale with increasing lead time; when lead time reaches 3 months, the spatial pattern correlation starts to fall below 0.5 (Fig. 8b). But, the spatial correlation skill appears to "bounce back" at an 8-month lead forecast. Due to data limitation, we are not able to determine to what extent this rebound lasts and whether this rebound is a robust feature.

Table 2 shows how the percentage variances accounted for by the first two major modes vary with the forecast lead time. For the first mode, the 0-month lead ensemble hindcast yields a quite realistic percentage variance (34%) compared to CMAP analysis (30%). However, the fractional variance increases as the forecast lead time increases. In the 8-month lead forecast, the first mode accounts for 47.3% of total variance, implying that the long-lead forecast tends to overstress the first leading mode while undervaluing the contributions from the higher modes. This also suggests that ENSO is the dominant source that can provide long-lead (8-month) A-AM predictability. For the second mode, the 1-month lead forecast also yields a realistic estimation of its fractional variance. Again, as the lead time increases, the fractional variance tends to increase slightly but is not monotonic.

Figure 10 shows the power spectra of the first two PCs as a function of lead time. Similar to the fractional
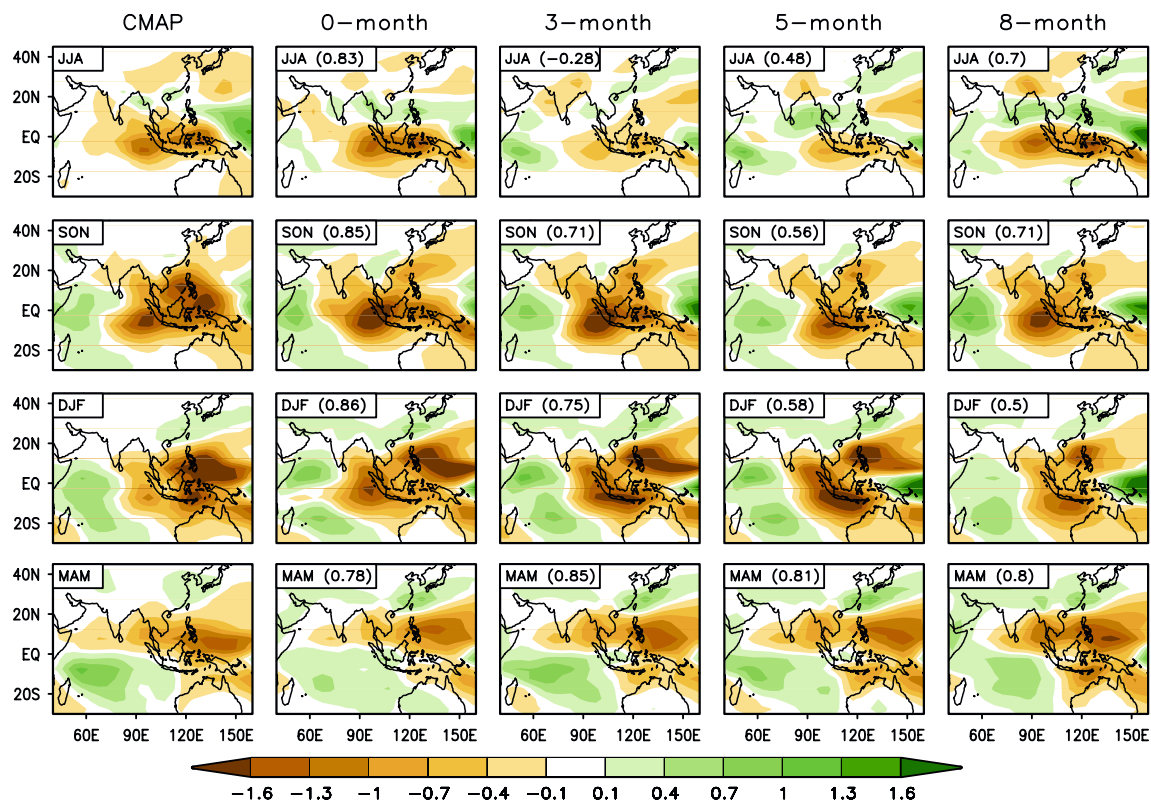
Fig. 9 Spatial patterns of the first S-EOF eigenvector of seasonal precipitation obtained from CMAP, and CFS seasonal forecast as a function of lead times of 0, 3, 5, and 8 months

Table 2 The percentage variances accounted for by the first two major modes as functions of the forecast lead time in CFS hindcast experiment

	CMAP	CFS retrospective forecasts as a functions of lead time				
		0-month	2-month	4-month	6-month	8-month
S-EOF 1	30.1	33.8	41.2	43.7	42.9	47.3
S-EOF 2	13.1	14.3	15.3	19.3	23.3	16.8

variance, the 0-month lead monthly ensemble hindcast yields realistic spectra for both PCs. The first PC has a double peak, with the major one occurring at 2–3 years and the second one at 5–6 years, while second PC has a peak at 5 years. As the lead time increases, the spectrum for the first mode loses the biennial peak quickly (Fig. 10, left panels), suggesting the biennial component of the A-AM is more difficult to predict than the LF component. This may be due in part to the coupled models' deficiencies in reproducing the biennial component of ENSO and due in part to the land surface memory that helps creating the biennial tendency but cannot maintain it for a long forecast lead. As the lead time increases, the power of the second mode substantially reduced after 4 months (Fig. 10, right panel).

6 Conclusion and discussion

6.1 Conclusion

Considering that the A-AM anomalies vary strongly with the seasons, a S-EOF analysis was adopted to depict the major modes of interannual variability. The S-EOF analysis of CMAP precipitation anomalies yielded two statistically distinguished modes, which account for about 30 and 13%, respectively, of the total variance of the interannual precipitation variation in the A-AM region. These two modes have distinct relationships with ENSO. The first mode concurs with the turnabout of warming to cooling in the eastern-central Pacific, whereas the second mode leads NINO 3.4 SST anomalies by about 1 year,
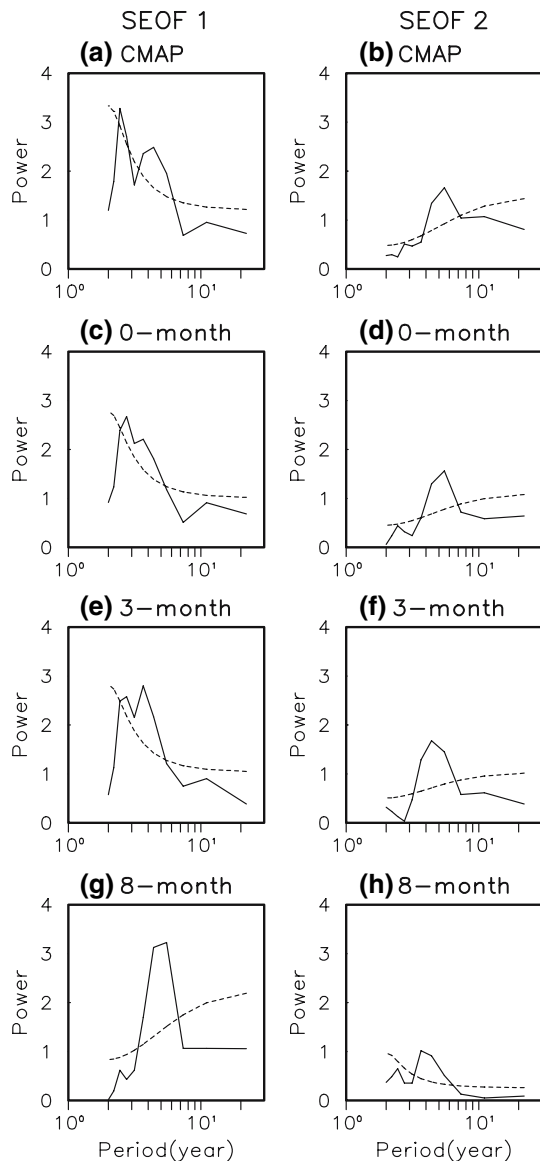
Fig. 10 The power spectrum density (*solid line*) and red noise (*dashed line*) of the first (*left-hand panels*) and the second (*right-hand panels*) S-EOF principal component of seasonal precipitation anomalies obtained from CMAP (**a**, **e**) lead time forecast and CFS 0-month (**b**, **f**), 3-month (**c**, **g**), and 8-month (**d**, **h**) lead time forecast

providing a precursor for El Niño/La Niña development (Fig. 2).

Ten coupled atmosphere–ocean–land climate models that participated DEMETER and APCC/CliPAS MME seasonal hindcast for the period of 1981–2001 have been evaluated against the observed leading modes of the A-AM precipitation. It was found that the 1-month lead seasonal hindcast of the MME captures realistic features of the spatial structure, seasonal evolution, and year-to-year variations, and the relationship with ENSO in terms of the first two leading modes of variability. The MME's second mode shows a potential to capture the precursors of ENSO

in the A-AM domain about five seasons prior to the maturation of a strong El Niño. Note that this does not imply that the MME can predict El Nino at a five-season lead. In summary, the current multi-coupled climate model ensemble prediction can faithfully predict the structure and temporal evolution of the two leading modes of variability, suggesting that the predictability arising from ENSO teleconnection and local monsoon–ocean interaction are captured by the models' MME.

However, the first two modes account for only 43% of the total variance. Further, the MME considerably underestimated the biennial tendency of the leading mode and the total variances accounted for by the first two modes. It is also found that during the decaying phase of ENSO, the models have deficiencies in capturing the austral fall monsoon precipitation over the maritime continent and the Walker-type teleconnection. This leads to a drop of prediction skill across the boreal spring.

The CFS hindcast experiments at NCEP provide a most comprehensive dataset for further analysis of the predictability of the two leading modes, varying with the forecast lead time. As the lead time increases, the fractional variance of the first mode increases, suggesting that the long-lead predictability comes primarily from ENSO predictability. The temporal correlation remains about 0.9 until the 6-month lead, when it drops significantly. The spatial pattern of the first mode exhibits a SPB in A-AM prediction, which is associated with the SPB in ENSO.

This study uncovered two surprising findings. First, the coupled models' MME 1-month lead seasonal predictions capture the first two leading modes of variability better than those captured by the ERA-40 and NCEP-2 reanalysis datasets (Fig. 5). Second, the results show that the CFS 1-month lead seasonal ensemble hindcast of the first leading modes is better than the MME in the amplitude of PC, the power spectra of the PCs, and the fractional variances.

6.2 Discussion

Given that the reanalysis datasets (ERA-40 and NCEP-2) are model assimilations forced by observed SST with observed data incorporated, how can the coupled climate model MME prediction of the first two leading modes be superior to the reanalysis? We argue that an important reason is that the MME includes ocean–atmosphere interaction processes, whereas the reanalysis data were obtained by forcing the atmospheric model with prescribed (observed) SST. In the reanalysis, although more realistic SST was used, the reanalysis procedure treated the atmosphere as a slave, thus neglecting the atmospheric feedback to the ocean. Treating the atmosphere as a slave may be inherently unable to simulate summer monsoon rainfall

variations in the heavily precipitating regions (Wang et al. 2004). Study of Kumar et al. (2005) demonstrated the superior prediction ability of a one-tier system over the corresponding two-tier system in predicting Indian subcontinent rainfall. Wu and Kirtman (2004) noted that local coupled air–sea feedback over the Indian Ocean plays an important role to simulate proper monsoon-ENSO relationship in dynamical model. The finding here concurs with the concept obtained from these previous studies. We believe that the coupled one-tier approach can enhance the predictability of the summer monsoon precipitation. Therefore, it is recommended that *future reanalysis should be carried out with coupled atmosphere and ocean models*.

While the MME in general better than any individual model, the CFS ensemble hindcast outperforms the MME in terms of the biennial tendency in the first mode and the amplitude of the anomalies, suggesting that the improved skill of MME prediction is at the expense of overestimating the fractional variance of the leading mode. These deficiencies partially limit the MME's predictive skill. The MME can only capture a portion of the precipitation variability.

The first mode has a strong biennial tendency and essentially reflects the Tropical Biennial Oscillation (TBO) (Meehl 1993). The result here suggests that the A-AM leading mode of interannual variability is an essential manifestation of the TBO and it provides a new perspective of the seasonally evolving spatio-temporal structure for TBO. The causes of this mode has been attributed to (1) remote ENSO forcing, (2) local monsoon–warm pool ocean interaction, and (3) the regulation of the powerful monsoon annual cycle (Wang et al. 2003). These processes are also essential for sustaining the TBO.

Of note is also that the first and second leading modes of Pacific-Indian Ocean SST are the LF mode and QB component, respectively, whereas the first and second A-AM leading modes are QB and LF modes, respectively. This suggests that while A-AM anomalies are influenced by ENSO, the intrinsic mechanisms within the A-AM system itself (such as monsoon–warm ocean interaction) also play a very important role in creating biennial tendency and modifying the response of the monsoon to ENSO.

A number of questions have been left without answers. The fact that the second S-EOF leads ENSO by 1 year suggests that monsoon anomalies may play a role in ENSO onset in the last two decades. However, the causes of the second important mode need to be explored further. In addition, which factors contribute to interannual predictability besides ENSO? Is there any additional source of predictability for A-AM precipitation prediction? The lack of understanding between the snow cover and monsoon predictability would be one of error source. These issues call for further investigation.

The current coupled climate models' prediction skill in the A-AM region remains moderate. There is substantial room for further improvements of the imperfect initial condition and models' representation of the real physics. Predictions over the land monsoon regions are particularly poor. We speculate that the poor land-surface initial conditions and the models' deficiencies in representing atmosphere-land interaction may be two of the major reasons for the MME's deficiency. There is an urgent need to determine to what extent improved land processes can contribute to better predictive skill.

References

Adler RF, Huffman GJ, Chang A, Ferraro R, Xie P, Janowiak J, Rudolf B, Schneider U, Curtis S, Bolvin D, Gruber A, Susskind J, Arkin P (2003) The version 2 global precipitation climatology project (GPCP) monthly precipitation analysis (1979-present). J Hydrometeor 4:1147–1167

Bengtsson L, Schlese U, Roeckner E, Latif M, Barnett TP, Graham NE (1993) A two-tiered approach to long-range climate forecasting. Science 261:1027–1029

Bjerknes J (1969) Atmospheric teleconnections from the equatorial Pacific. Mon Weather Rev 97:163–172

Cane MA, Zebiak SE, Dolan SC (1986) Experimental forecasts of El Niño. Nature 321:827–832

Delecluse P, Madec G (1999) Ocean modeling and the role of the ocean in the climate system. In: Holland WR, Joussaume S, David F (eds) Modeling the earth's climate and its variability, Les Houches 1997. Elsevier Science, Amsterdam

Deque M (2001) Seasonal predictability of tropical rainfall: probabilistic formulation and validation. Tellus 53A:500–512

Doblas-Reyes FJ, Deque M, Piedelievre J-P (2000) Multi-model spread and probabilistic seasonal forecasts in PROVOST. Q J R Meteorol Soc 126:2069–2088

Gadgil S, Sajani S (1998) Monsoon precipitation in the AMIP runs. Clim Dyn 14:659–689

Gordon C, Cooper C, Senior CA, Banks HT, Gregory JM, Johns TC, Mitchell JFB, Wood RA (2000) Simulation of SST, sea ice extents and ocean heat transports in a version of the Hadley Centre coupled model without flux adjustments. Clim Dyn 16:147–168

Goswami BN (1998) Interannual variations of Indian summer monsoon in a GCM: external conditions versus internal feedbacks. J Clim 11:501–522

Gregory D, Morcrette JJ, Jakob C, Beljaars ACM, Stockdale T (2000) Revision of convection, radiation and cloud schemes in the ECMWF Integrated Forecasting System. Q J R Meteorol Soc 126:1685–1710

Hung CW, Liu X, Yanai M (2004) Symmetry and asymmetry of the Asian and Australian summer monsoon. J Clim 17:2413–2426

Kanamitsu M, Ebisuzaki W, Woollen J, Yang S-K, Hnilo JJ, Fiorino M, Potter GL (2002) NCEP-DOE AMIP-II reanalysis (R-2). Bull Am Meteorol Soc 83:1631–1643

Kim KY (2002) Investigation of ENSO variability using cyclostationary EOFs of observational data. Meteorol Atmos Phys 81:149–168

Krishnamurti TN, Kishtawal CM, Zhang Z, LaRow TE, Bachiochi DR, et al (1999) Improved weather and seasonal climate forecasts from multi-model superensemble. Science 285:1548–1550

Kug JS, Kang I-S (2007) Seasonal climate prediction with SNU tier-one and tier-two prediction systems. Clim Dyn (in press)

Kumar KK, Hoerling M, Rajagopalan B (2005) Advancing Indian monsoon rainfall predictions. Geophys Res Lett 32:L08704

Lorenz EN (1965) A study of the predictability of a 28-variable model. Tellus 17:321–333

Luo J-J, Masson S, Behera S, Shingu S, Yamagata T (2005) Seasonal climate predictability in a coupled OAGCM using a different approach for ensemble forecasts. J Clim 18:4474–4497

Madec G, Delecluse P, Imbrad M, Levy C (1997) OPA release 8, ocean general circulation model reference manual. Internal report, LODYC, Paris

Madec G, Delecluse P, Imbrad M, Levy C (1998) OPA version 8.1, ocean general circulation model reference manual. Technical report no. 11, LODYC, Paris

Marsland SJ, Haak H, Jungclaus J-H, Latif M, Roske F (2003) The Max-Planck-Institute global ocean/sea ice model with orthogonal curvilinear coordinates. Ocean Model 5:91–127

Meehl GA (1987) The annual cycle and interannual variability in the tropical Pacific and Indian Ocean regions. Mon Weather Rev 115:27–50

Meehl GA (1993) A coupled air-sea biennial mechanism in the tropical Indian and Pacific regions: role of the ocean. J Clim 6:31–41

North GR, Bell TL, Cahalan RF, Moeng FJ (1982) Sampling errors in the estimation of empirical orthogonal functions. Mon Weather Rev 110:699–706

Palmer TN, Brankovic C, Richardson DS (2000) A probability and decision-model analysis of PROBOST seasonal multi-model ensemble integrations. Q J R Meteorol Soc 126:2013–2034

Palmer TN, Alessandri A, Andersen U, Cantelaube P, Davey M, et al (2004) Development of a European multi-model ensemble system for seasonal to interannual prediction (DEMETER). Bull Am Meteorol Soc 85:853–872

Pope VD, Gallani ML, Rowntree PR, Stratton RA (2000) The impact of new physical parameterizations in the Hadley Centre climate model: HadAM3. Clim Dyn 16:123–146

Rasmussen EM, Carpenter TH (1982) Variations in tropical sea surface temperature and surface wind fields associated with the Southern Oscillation/El Nino. Mon Weather Rev 110:354–384

Roeckner E, Arpe K, Bengtsson L, Christoph M, Claussen M, Dumenil L, Esch M, Giorgetta M, Schlese U, Schulzweida U (1996) The atmospheric general circulation model ECHAM4: model description and simulation of present-day climate. Report no. 218, Max Planck Institut fur Meteorologie, Hamburg

Rowell DP, Folland CK, Maskell K, Ward MN (1995) Variability of summer rainfall over tropical North Africa (1906–92): observations and modeling. Q J R Meteorol Soc 121:669–704

Saha S, Nadiga S, Thiaw C, Wang J, et al (2006) The NCEP climate forecast system. J Clim 19:3483–3517

Saji HN, Goswami BN, Vinayachandran PN, Yamaghata T (1999) A dipole mode in the tropical Indian Ocean. Nature 401:360–363

Shukla J (1981) Dynamical predictability of monthly means. J Atmos Sci 38:2547–2572

Shukla J, et al (2000) Dynamical seasonal prediction. Bull Am Meteorol Soc 81:2493–2606

Smith TM, Reynolds RW (2004) Improved extended reconstruction of SST (1854–1997). J Clim 17:2466–2477

Sperber KR, Palmer TN (1996) Interannual tropical rainfall variability in general circulation model simulations associated with the Atmospheric Model Intercomparison Project. J Clim 9:2727–2750

Turner AG, Inness PM, Slingo JM (2005) The role of the basic state in the ENSO-monsoon relationship and implications for predictability. Q J R Meteorol Soc 131:781–804

Uppala SM, Kållberg PW, Simmons AJ, Andrae U, da Costa Bechtold V, et al (2005) The ERA-40 re-analysis. Q J R Meteorol Soc 131:2961–3012

Wang B (1995) Interdecadal changes in El Nino onset in the last four decades. J Clim 8:267–285

Wang B, An SI (2005) A method for detecting season-dependent modes of climate variability: S-EOF analysis. Geophys Res Lett 32:L15710. doi:10.1029/2005GL022709

Wang B, Wu R, Li T (2003) Atmosphere-warm ocean interaction and its impact on Asian–Australian monsoon variation. J Clim 16:1195–1211

Wang B, Kang I-S, Lee J-Y (2004) Ensemble simulations of Asian–Australian monsoon variability by 11 AGCMs. J Clim 17:803–818

Wang B, Ding QH, Fu XH, Kang I-S, Jin K, Shukla J, Doblas-Reyes F (2005) Fundamental challenge in simulation and prediction of summer monsoon rainfall. Geophys Res Lett 32:L15711

Wang B, Yang J, Zhou T, Wang B (2007a) Interdecadal changes in major modes of Asian-Australian monsoon interannual variability. Clim Dyn (in press)

Wang B, Lee J-Y, Kang I-S, Shukla J et al (2007b) Assessment of the APCC/CliPAS multi-model seasonal hindcast. Clim Dyn (Submitted)

Weare BC, Nasstrom JS (1982) Examples of extended empirical orthogonal function analyses. Mon Weather Rev 110:481–485

Webster PJ, Yang S (1992) Monsoon and ENSO: selectively interactive system. Q J R Meteorol Soc 118:877–926

Webster PJ, Moore AM, Loschnigg JP, Leben RR (1999) Coupled ocean-atmosphere dynamics in the Indian Ocean during 1997–1998. Nature 401:356–360

Wolff JE, Maier-Reimer E, Legutke S (1997) The Hamburg Ocean primitive equation model. Technical report no. 13, Deutsches Klimarechenzentrum, Hamburg

Wu R, Kirtman B (2004) Impacts of the Indian Ocean on the Indian summer monsoon-ENSO relationship. J Clim 17:3037–3054

Wu R, Kirtman B (2005) Roles of Indian and Pacific Ocean air-sea coupling in tropical atmospheric variability. Clim Dyn 25:155–170

Xie P, Arkin PA (1997) Global precipitation: a 17-year monthly analysis based on gauge observations, satellite estimates, and numerical model outputs. Bull Am Meteorol Soc 78:2539–2558

Yasunari T (1991) The monsoon year—a new concept of the climatic year in the tropics. Bull Am Meteorol Soc 72:1331–1338

Zebiak SE, Cane MA (1987) A model of El Niño-Southern Oscillation. Mon Weather Rev 115:2262–2278